

INVERSE COMPTON X-RAY EMISSION FROM SUPERNOVAE WITH COMPACT PROGENITORS: APPLICATION TO SN2011FE

R. MARGUTTI¹, A. M. SODERBERG¹, L. CHOMIUK^{1,2}, R. CHEVALIER³, K. HURLEY⁴, D. MILISAVLJEVIC¹, R. J. FOLEY^{1,21}, J. P. HUGHES⁵, P. SLANE¹, C. FRANSSON⁶, M. MOE¹, S. BARTHELMEY⁷, W. BOYNTON⁸, M. BRIGGS⁹, V. CONNAUGHTON⁹, E. COSTA¹⁰, J. CUMMINGS⁷, E. DEL MONTE¹⁰, H. ENOS⁸, C. FELLOWS⁸, M. FEROCI¹⁰, Y. FUKAZAWA¹¹, N. GEHRELS⁷, J. GOLDSTEN¹², D. GOLOVIN¹³, Y. HANABATA¹¹, K. HARSHMAN⁸, H. KRIMM⁷, M. L. LITVAK¹³, K. MAKISHIMA¹⁴, M. MARISALDI¹⁵, I. G. MITROFANOV¹³, T. MURAKAMI¹³, M. OHNO¹¹, D. M. PALMER¹⁷, A. B. SANIN¹³, R. STARR⁷, D. SVINKIN¹⁸, T. TAKAHASHI¹¹, M. TASHIRO¹⁹, Y. TERADA¹⁹, K. YAMAOKA²⁰

(Dated: Accepted YEAR month day. Received YEAR month day; in original form YEAR month day)
Draft version February 7, 2018

ABSTRACT

We present a generalized analytic formalism for the inverse Compton X-ray emission from hydrogen-poor supernovae and apply this framework to SN 2011fe using Swift-XRT, UVOT and Chandra observations. We characterize the optical properties of SN 2011fe in the Swift bands and find them to be broadly consistent with a “normal” SN Ia, however, no X-ray source is detected by either XRT or Chandra. We constrain the progenitor system mass loss rate $\dot{M} < 2 \times 10^{-9} M_{\odot} \text{yr}^{-1}$ (3σ c.l.) for wind velocity $v_w = 100 \text{ km s}^{-1}$. Our result rules out symbiotic binary progenitors for SN 2011fe and argues against Roche-lobe overflowing subgiants and main sequence secondary stars if $\gtrsim 1\%$ of the transferred mass is lost at the Lagrangian points. Regardless of the density profile, the X-ray non-detections are suggestive of a clean environment ($n_{CSM} < 150 \text{ cm}^{-3}$) for $2 \times 10^{15} \lesssim R \lesssim 5 \times 10^{16} \text{ cm}$ around the progenitor site. This is either consistent with the bulk of material being confined within the binary system or with a significant delay between mass loss and supernova explosion. We furthermore combine X-ray and radio limits from Chomiuk et al. 2012 to constrain the post shock energy density in magnetic fields. Finally, we searched for the shock breakout pulse using gamma-ray observations from the Interplanetary Network and find no compelling evidence for a supernova-associated burst. Based on the compact radius of the progenitor star we estimate that the shock break out pulse was likely not detectable by current satellites.

Subject headings: radiation mechanisms: non thermal

¹ Harvard-Smithsonian Center for Astrophysics, 60 Garden St., Cambridge, MA 02138, USA.

² National Radio Astronomy Observatory, P. O. Box O Socorro, NM 87801, USA.

³ Department of Astronomy, University of Virginia, Charlottesville, VA 22904-4325, USA.

⁴ Space Sciences Laboratory, University of California, 7 Gauss Way, Berkeley, CA 94720-7450, USA.

⁵ Department of Physics and Astronomy, Rutgers University, Piscataway, NJ 08854-8019, USA.

⁶ Department of Astronomy, Stockholm University, AlbaNova, SE-106 91 Stockholm, Sweden.

⁷ NASA/Goddard Space Flight Center Greenbelt, MD 20771, USA.

⁸ Department of Planetary Sciences, University of Arizona, Tucson, AZ 85721, USA.

⁹ Physics Department, The University of Alabama in Huntsville, Huntsville, AL 35809, USA.

¹⁰ INAF/IASF-Roma, via Fosso del Cavaliere 100, 00133 Roma, Italy.

¹¹ Department of Physics, Hiroshima University, 1-3-1 Kagamiyama, Higashi-Hiroshima, Hiroshima 739-8526, Japan.

¹² Applied Physics Laboratory, Johns Hopkins University, Laurel, MD 20723, USA.

¹³ Space Research Institute, 84/32, Profsoyuznaya, Moscow 117997, Russian Federation.

¹⁴ Department of Physics, University of Tokyo, 7-3-1 Hongo, Bunkyo-ku, Tokyo 113-0033, Japan.

¹⁵ INAF/IASF-Bologna, Via Gobetti 101, I-40129 Bologna, Italy.

¹⁶ Department of Physics, Kanazawa University, Kadoma-cho, Kanazawa, Ishikawa 920-1192, Japan.

¹⁷ Los Alamos National Laboratory, P.O. Box 1663, Los Alamos, NM 87545, USA.

¹⁸ Ioffe Physical-Technical Institute of the Russian Academy of Sciences, St. Petersburg, 194021, Russia.

¹⁹ Department of Physics, Saitama University, 255 Shimo-Okubo, Sakura-ku, Saitama-shi, Saitama 338-8570, Japan.

²⁰ Department of Physics and Mathematics, Aoyama Gakuin University, 5-10-1 Fuchinobe, Sagami-hara, Kanagawa 229-8558, Japan.

²¹ Clay Fellow.

1. INTRODUCTION

Over the past two decades, the utility of Type Ia supernovae (SNe Ia) as standardizable candles to trace the expansion history of the Universe has been underscored by the increasing resources dedicated to optical/near-IR discovery and follow-up campaigns (Riess et al. 1998; Perlmutter et al. 1999). At the same time, the nature of their progenitor system(s) has remained elusive, despite aggressive studies to unveil them (see e.g. Hillebrandt & Niemeyer 2000). The second nearest Ia SN discovered in the digital era, SN 2011fe (Nugent et al. 2011b) located at $d_L = 6.4$ Mpc (Shappee & Stanek 2011), represents a natural test bed for a detailed SN Ia progenitor study²². The best studied Type Ia SN at early times before SN 2011fe, SN 2009ig, demonstrated how single events can provide significant insight into the properties of this class of explosions (Foley et al. 2012).

The fundamental component of SN Ia progenitor models is an accreting white dwarf (WD) in a binary system. Currently, the most popular models include (i) a single-degenerate (hereafter, SD) scenario in which a massive WD accretes material from a H-rich or He-rich companion, potentially a giant, sub-giant or main-sequence star, (Whelan & Iben 1973; Nomoto 1980). Mass is transferred either via Roche-lobe overflow (RLOF) or through stellar winds. Alternatively, (ii) models invoke a double sub- M_{Ch} WD binary system that eventually merges (double degenerate model, DD; Iben & Tutukov 1984, Webbink 1984).

In SD models, the circumbinary environment may be enriched by the stellar wind of the donor star or through non-conservative mass transfer in which a small amount of material is lost to the surroundings. Winds from the donor star shape the local density profile as $\rho_{CSM} \propto R^{-2}$ over a $\lesssim 1$ parsec region encompassing the binary system. Theoretical considerations indicate that the wind-driven mass loss rate must be low, since an accretion rate of just $\sim 3 \times 10^{-7} M_{\odot} \text{ yr}^{-1}$ is ideal for the WD to grow slowly up to M_{Ch} and still avoid mass-losing nova eruptions (steady burning regime, Nomoto et al. 1984). Strong evidence for the *lack* of a wind-stratified medium and/or the detection of a constant local density (with a typical interstellar medium density of $n_{CSM} \approx 0.1 - 1 \text{ cm}^{-3}$) may instead point to a DD model.

Arising from the interaction of the SN shock blast wave with the circumbinary material, radio and X-ray observations can potentially discriminate between the two scenarios by shedding light on the properties of the environment, shaped by the evolution of the progenitor system (see e.g. Boffi & Branch 1995, Eck et al. 1995). Motivated thus, several dozen SNe Ia at distances $d \lesssim 200$ Mpc have been observed with the Very Large Array (VLA; Panagia et al. 2006; Hancock et al. 2011; Soderberg in prep.), the Chandra X-ray Observatory (Hughes et al. 2007), and the Swift X-ray Telescope (Immler et al. 2006; Russel & Immler, in press) revealing no detections to date²³. These limits were used to constrain the density of the circumbinary material, and in turn the mass loss rate of the progenitor system. However these data poorly constrain the WD companion, due in part to the limited sensitivity of the observations (and the distance of the SNe).

²² The nearest Type Ia in the digital era is SN 1986G which exploded in NGC 5128 at a distance of ~ 4 Mpc (Frogel et al. 1987).

²³ We note that the claimed detection of SN 2005ke with the *Swift*-XRT was not confirmed with follow-up Chandra observations, strongly suggesting that the *Swift*/XRT source was due to contamination from the host galaxy (Hughes et al. 2007).

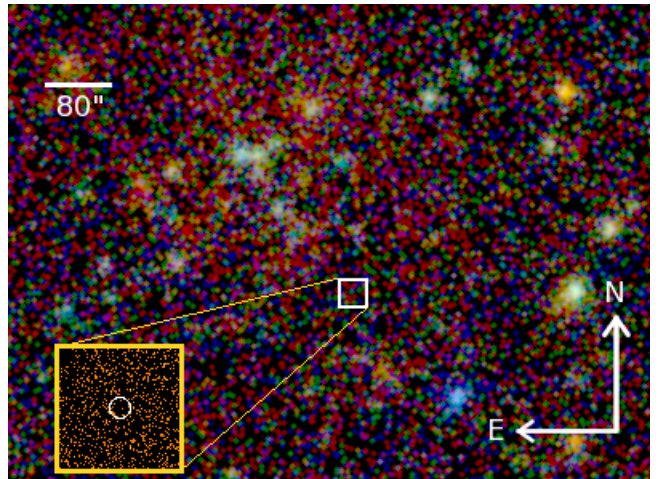


FIG. 1.— *Swift*-XRT color combined image of the environment around SN 2011fe. Red, green and blue colors refer to soft (0.3-1 keV), medium (1-3 keV) and hard (3-10 keV) sources, respectively. A 40" region around the SN is marked with a white box. Inset: *Chandra* 0.5-8 keV deep observation of the same region obtained at day 4 since the explosion. No source is detected at the SN position (white circle).

The improved sensitivity of the Expanded Very Large Array (EVLA) coupled with a more detailed approach regarding the relevant radio and X-ray emission (and absorption) processes in Type Ia supernovae, has enabled the deepest constraints to date on a circumbinary progenitor as discussed in our companion paper on the recent Type Ia SN 2011fe/PTF11kly (Chomiuk et al. 2012. See also Horesh et al. 2011).

Here we report a detailed panchromatic study of SN 2011fe bridging optical/UV and gamma-ray observations. Drawing from observations with the *Swift* and Chandra satellites as well as the Interplanetary Network (IPN; Hurley 2010), we constrain the properties of the bulk ejecta and circumbinary environment through a self-consistent characterization of the dynamical evolution of the shockwave. First we present optical/UV light-curves for the SN, indicating that the object appears consistent with a "normal" SN Ia. Next we discuss deep limits on the X-ray emission in the month following explosion. We furthermore report gamma-ray limits (25-150 keV) for the shock breakout pulse. In the Appendix we present an analytic generalization for the the Inverse Compton (IC) X-ray luminosity expected from hydrogen poor SNe that builds upon previous work by Chevalier & Fransson 2006 and Chevalier et al. 2006 but is broadly applicable for a wide range of shock properties, metallicity, photon temperatures, and circumstellar density profiles (stellar wind or ISM; see Appendix A). We apply this analytic model to SN 2011fe to constrain the density of the circumbinary environment, and find that our limits are a factor of ~ 10 deeper than the results recently reported by Horesh et al. 2011.

Observations are described in Sec. 2; limits to the SN progenitor system from X-ray observations are derived and discussed in Sec. 3 using the IC formalism from Appendix A. We combine our radio (Chomiuk et al. 2012) and X-ray limits to constrain the post-shock energy density in magnetic fields in Sec. 4, while the results from the search of a burst of gamma-ray radiation from the SN shock break-out is presented in Sec. 5. Conclusions are drawn in Sec. 6.

2. OBSERVATIONS

SN 2011fe was discovered by the Palomar Transient Factory (PTF) on 2011 August 24.167 UT and soon identified

as a very young type Ia explosion in the Pinwheel galaxy (M101) (Nugent et al. 2011a). From early time optical observations Nugent et al. (2011b) were able to constrain the SN explosion date to August 23, 16 : 29 ± 20 min (UT). The SN site was fortuitously observed both by the *Hubble Space Telescope* (HST) and by *Chandra* on several occasions prior to the explosion in the optical and X-ray band, giving the possibility to constrain the progenitor system (Li et al. 2011a; Liu et al. 2011). Very early optical and UV photometry has been used by Brown et al. (2011) and Bloom et al. (2011) to infer the progenitor and companion radius and nature, while multi-epoch high-resolution spectroscopy taken during the evolution of the SN has been employed as a probe of the circumstellar environment (Patat et al. 2011b). Limits to the circumstellar density have been derived from deep radio observations in our companion paper (Chomiuk et al. 2012), where we consistently treat the shock parameters and evolution. Here we study SN 2011fe from a complementary perspective, bridging optical/UV, X-ray and gamma-ray observations.

Swift observations were acquired starting from August 24, 1.25 days since the onset of the explosion. *Swift*-XRT data have been analyzed using the latest release of the HEASOFT package at the time of writing (v11). Standard filtering and screening criteria have been applied. No X-ray source consistent with the SN position is detected in the 0.3–10 keV band either in promptly available data (Horesh et al. 2011; Margutti & Soderberg 2011b) or in the combined 142 ks exposure covering the time interval 1–65 days (see Fig. 1). In particular, using the first 4.5 ks obtained on August 24th, we find a PSF (Point Spread Function) and exposure map corrected²⁴ 3σ count-rate limit on the undetected SN $\lesssim 4 \times 10^{-3} \text{ cs}^{-1}$. For a simple power-law spectrum with photon index $\Gamma \sim 2$ and Galactic neutral hydrogen column density $N_{\text{H}} = 1.8 \times 10^{20} \text{ cm}^{-2}$ (Kalberla et al. 2005) this translates into an unabsorbed 0.3–10 keV flux $F = 1.5 \times 10^{-13} \text{ erg s}^{-1} \text{ cm}^{-2}$ corresponding to a luminosity $L = 7 \times 10^{38} \text{ erg s}^{-1}$ at a distance of 6.4 Mpc (Shappee & Stanek 2011). Collecting data between 1 and 65 days after the explosion (total exposure of 142 ks) we obtain a 3σ upper limit of $2 \times 10^{-4} \text{ cs}^{-1}$ ($F = 7.4 \times 10^{-15} \text{ erg s}^{-1} \text{ cm}^{-2}$, $L = 3.6 \times 10^{37} \text{ erg s}^{-1}$). Finally, extracting data around maximum light (the time interval 8–38 days), the X-rays are found to contribute less than $3 \times 10^{-4} \text{ cs}^{-1}$ (3σ limit, total exposure of 61 ks) corresponding to $F = 1.1 \times 10^{-14} \text{ erg s}^{-1} \text{ cm}^{-2}$, $L = 5.9 \times 10^{37} \text{ erg s}^{-1}$.

We observed SN 2011fe with the *Chandra* X-ray Observatory on Aug 27.44 UT (day 4 since the explosion) under an approved DDT proposal (PI Hughes). Data have been reduced with the CIAO software package (version 4.3), with calibration database CALDB (version 4.4.2). We applied standard filtering using CIAO threads for ACIS data. No X-ray source is detected at the SN position during the 50 ks exposure (Hughes et al. 2011), with a 3σ upper limit of $1.1 \times 10^{-4} \text{ cs}^{-1}$ in the 0.5–8 keV band, from which we derive a flux limit of $7.7 \times 10^{-16} \text{ erg s}^{-1} \text{ cm}^{-2}$ corresponding to $L = 3.8 \times 10^{36} \text{ erg s}^{-1}$ (assuming a simple power-law model with spectral photon index $\Gamma = 2$). 3σ upper limits from *Swift* and *Chandra* observations are shown in Fig. 2.

The SN was clearly detected in *Swift*-UVOT observations. Photometry was extracted from a $5''$ aperture, closely follow-

ing the prescriptions by Brown et al. (2009) (see Fig. 2). Pre-explosion images of the host galaxy acquired by UVOT in 2007 were used to estimate and subtract the host galaxy light contribution. Our photometry agrees (within the uncertainties) with the results of Brown et al. (2011). With respect to Brown et al. (2011) we extend the UVOT photometry of SN 2011fe to day ~ 60 since the explosion. Due to the brightness of SN 2011fe, u, b and v observations strongly suffer from coincidence losses (Breeveld et al. 2010) around maximum light (see Brown et al. 2011 for details): supernova templates from Nugent et al. (2002) were used to fit the u and b light-curves and infer the SN luminosity during those time intervals in the u and b bands. For the v-band, it was possible to (partially) recover the original light-curve applying standard coincidence losses corrections: however, due to the extreme coincidence losses, our v-band light-curve may still provide a lower limit to the real SN luminosity in the time interval 8–37 days since explosion. In Fig. 2 we present the *Swift*-UVOT 6-filter light-curves, and note that the re-constructed v-band is broadly consistent with the Nugent template²⁵. We adopted a Galactic reddening of $E(B-V) = 0.01$ (Schlegel et al. 1998).

In the case of the "golden standard" Ia SN 2005cf (which is among the best studied Ia SNe), the V band is found to contribute $\sim 20\%$ to the bolometric luminosity (Wang et al. 2009), with limited variation over time. For SN 2011fe, we measure at day 4 a v-band luminosity $L_{\text{v}} \sim 10^{41} \text{ erg s}^{-1}$, corresponding to $L_{\text{bol}} \approx 5 \times 10^{41} \text{ erg s}^{-1}$ and note that at this time the luminosity in the v, b, u, w1 and w2 bands account for $\approx 0.5 L_{\text{bol}}$. We therefore assumed that the v, b, u, w1 and w2 bands represent²⁶ $\approx 0.5 L_{\text{bol}}$. In the following we explicitly provide the dependence of our density limits on L_{bol} , so that it is easily possible to re-scale our limits to any L_{bol} value. Given that the optical properties point to a normal SN Ia (Parrent et al. in prep.) we adopt fiducial parameters $M_{\text{ej}} = 1.4 M_{\odot}$ and $E = 10^{51} \text{ erg}$ for the ejecta mass and SN energy, respectively, throughout this paper.

3. LIMITS ON THE AMBIENT DENSITY FROM X-RAYS

X-ray emission from SNe may be attributed to a number of emission processes including (i) synchrotron, (ii) thermal, (iii) Inverse Compton (IC), or (iv) a long-lived central engine (see Chevalier & Fransson 2006 for a review). It has been shown that the X-ray emission from stripped supernovae exploding into low density environments is dominated by IC on a timescale of weeks to a month since explosion, corresponding to the peak of the optical emission (Björnsson & Fransson 2004, Chevalier & Fransson 2006). In specific cases, this has been shown to be largely correct (e.g., SN 2008D Soderberg et al. 2008, SN 2011dh Soderberg et al. 2011).

In this framework the X-ray emission is originated by up-scattering of optical photons from the SN photosphere by a population of relativistic electrons (e.g. Björnsson & Fransson 2004). The IC X-ray luminosity depends on the density structure of the SN ejecta, the structure of the circumstellar medium (CSM) and the details of the relativistic electron distribution responsible for the up-scattering. Here we assume the SN outer density structure

²⁵ Note that, as it will be clear from the next section, this possible underestimation of the v-band luminosity around maximum light only leads to more conservative limits to the ambient density derived from *Swift* observations. Our main conclusions are however based on the *Chandra* observation taken at day 4, when coincidence losses do not play a role.

²⁶ Nearly 80% of the bolometric luminosity of a typical SN Ia is emitted in the range from 3000 to 10000 Å (Contardo et al. 2000).

²⁴ Note that correcting for both the PSF and the exposure map is here of primary importance to compute the upper limits. If the exposure map is neglected, deeper but unrealistic limits would be computed.

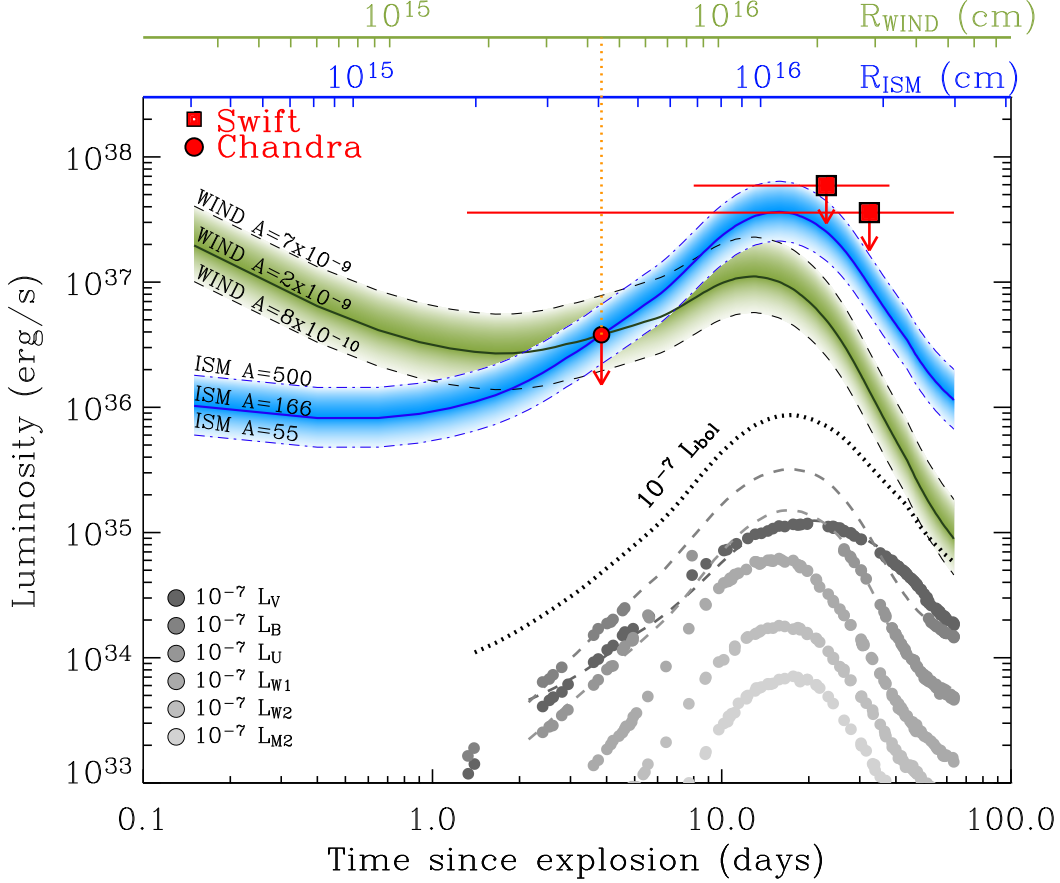


FIG. 2.— Limits on the X-ray luminosity of SN 2011fe: 0.5–8 keV luminosity expected from inverse Comptonization of optical photons in the case of a wind $\rho_{CSM} \propto R^{-2}$ (green solid line) and an ISM $\rho_{CSM} \propto \text{const}$ (blue solid line) environment. Deep limits from *Swift* and *Chandra* are marked with red bullets and squares, respectively. In the case of *Swift* observations we report the combined limit (at the linear midpoint of the time intervals), produced stacking the entire *Swift*-XRT data set together with a limit calculated around the SN maximum light. The colored areas span $A = (0.8 - 7) \times 10^{-9} M_{\odot} \text{yr}^{-1} / (100 \text{ km s}^{-1})$ (wind, green) and $A = (55 - 500) \text{ cm}^{-3}$ (ISM, blue). The *Chandra* observation constrains $\dot{M}/v_w < 2 \times 10^{-9} M_{\odot} \text{yr}^{-1} / (100 \text{ km s}^{-1})$ (wind); $n_{CSM} < 166 \text{ cm}^{-3}$ (ISM). The blue and green x-axes report the ISM and wind radius of the shock calculated using these values. Black dotted line: scaled SN bolometric luminosity. Grey filled circles: scaled *Swift*-UVOT light-curves. Dashed lines: best-fitting Nugent et al. (2002) templates to the u b and v band. We assume $E = 10^{51} \text{ erg}$, $M_{ej} = 1.4 M_{\odot}$, $\epsilon_e = 0.1$, $p = 3$.

$\rho_{SN} \propto R^{-n}$ with $n \sim 10$ (Chevalier & Fransson 2006), as found for SNe arising from compact progenitors (as a comparison, Matzner & McKee 1999 found the outermost profile of the ejecta to scale as $\rho_{SN} \propto R^{-10.2}$. See Chomiuk et al. 2012, Soderberg in prep. for a discussion)²⁷; the SN shock propagates into the circumstellar medium and is assumed to accelerate the electrons in a power-law distribution $n_e(\gamma) = n_0 \gamma^{-p}$ for $\gamma > \gamma_{\min}$. Radio observations of type Ib/c SNe indicate $p \sim 3$ (Chevalier & Fransson 2006). However, no radio detection has ever been obtained for a type Ia SN so that the value of p is currently unconstrained: this motivates us to explore a wider parameter space $p \gtrsim 2.1$ (Fig. 3) as seen for mildly relativistic and relativistic explosions (e.g., gamma-ray bursts, Panaitescu & Kumar 2000; Yost et al. 2003; Curran et al. 2010). Finally, differently from the thermal or synchrotron mechanisms, the IC luminosity is directly related to the bolometric luminosity of the SN ($L_{IC}(t) \propto L_{bol}(t)$): the environment directly determines the *ratio* of the optical to the X-ray

²⁷ Note that the adopted density profile is similar to the W7 model by Nomoto et al. (1984) with the addition of a power-law profile at high velocities. A pure W7 profile would give rise to somewhat slower shockwave velocity (Dwarkadas & Chevalier 1998).

luminosity, so that possible uncertainties on the distance of the SN do not affect the IC computation; it furthermore does *not* require any assumption on magnetic field related parameters.

For a population of optical photons with effective temperature T_{eff} , the IC luminosity at frequency ν reads (see Appendix A):

$$\frac{dL_{IC}}{d\nu} \sim 0.2 \left(\frac{h}{3.6k} \right)^{\frac{3-p}{2}} \frac{(p-2) \sigma_T \epsilon_e \rho_{CSM} v_s^2 \gamma_{\min}^{(p-2)} T_{\text{eff}}^{\frac{p-3}{2}} \nu^{\frac{1-p}{2}} \Delta R}{m_e c^2} L_{bol}(t) \quad (1)$$

where ΔR is the extension of the region containing fast electrons; ρ_{CSM} is the circumstellar medium density the SN shock is impacting on, which we parametrize as a power-law in shock radius $\rho_{CSM} \propto R^{-s}$; together with ρ_{SN} , ρ_{CSM} determines the shock dynamics, directly regulating the evolution of the shock velocity $v_s \equiv v_s(t, n, s)$, shock radius $R \equiv R(t, n, s)$ and $\gamma_{\min} \equiv \gamma_{\min}(t, n, s)$ as derived in Appendix A. For the special case $p = 3$, $\frac{dL_{IC}}{d\nu} \propto \nu^{-1}$, its dependence on T_{eff} cancels out and it is straightforward to verify that Eq. 1 matches the predictions from Chevalier & Fransson (2006), their Eq. (31) for $s = 2$ (wind medium). In the following we use Eq. 1 and the

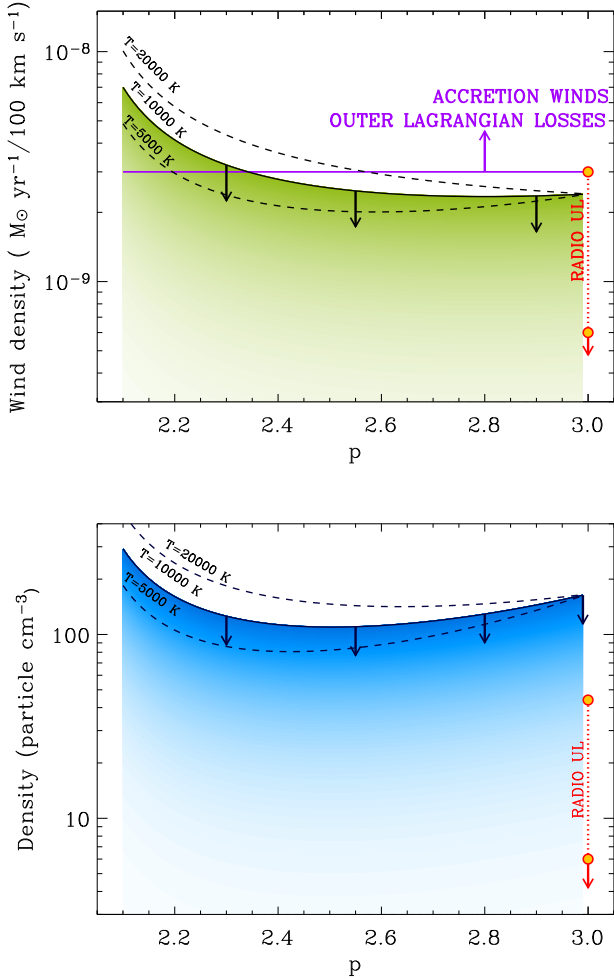


FIG. 3.— Limits on the CSM density around SN 2011fe as derived from the X-ray non-detection at 4 days after the explosion, assuming inverse comptonization of optical photons in the case of a wind (upper panel) or ISM (lower panel) scenario. Black solid line: 3σ upper limit as a function of the power-law index of the electron distribution p assuming $T = 10000$ K. Upper limit contours in the cases $T = 5000$ K and $T = 20000$ K are also shown for comparison (black dashed lines). Yellow bullets: upper limit to the CSM density as derived from radio observations for ϵ_B in the range 0.1–0.01. $\epsilon_B = 0.1$ gives the tightest constraint (Chomiuk et al. 2012). We assume $E = 10^{51}$ erg, $M_{ej} = 1.4M_{\odot}$, $\epsilon_e = 0.1$.

$L_{bol}(t)$ evolution calculated from *Swift*-UVOT observations of SN 2011fe (Sec. 2) to derive limits on the SN environment assuming different density profiles. We assume $\epsilon_e = 0.1$, as indicated by well studied SN shocks (Chevalier & Fransson 2006). Each limit on the environment density we report below has to be re-scaled of a multiplicative factor $(0.1/\epsilon_e)^{(p-1)}$ for other ϵ_e values.

3.1. Wind scenario

A star which has been losing material at constant rate \dot{M} gives rise to a "wind medium": $\rho_{CSM} = \dot{M}/(4\pi R^2 v_w)$. Eq. A8 and the *Chandra* non-detection constrain the wind density to $\dot{M}/v_w < 2 \times 10^{-9} (M_{\odot} \text{yr}^{-1}/100 \text{km s}^{-1})$ (where v_w is the wind velocity). This is a 3σ limit obtained integrating Eq. A8 over the 0.5–8 keV *Chandra* pass band and assuming $p = 3$, $\epsilon_e = 0.1$, $E = 10^{51}$ erg and $M_{ej} = 1.4M_{\odot}$. The observation was performed on day 4 after the explosion: at this time $L_{bol} \sim 5 \times 10^{41}$ erg s^{-1} while the shock wave probes the en-

vironment density at a radius $R \sim 4 \times 10^{15}$ cm (Eq. A3 and A7) for $\dot{M}/v_w = 2 \times 10^{-9} (M_{\odot} \text{yr}^{-1}/100 \text{km s}^{-1})$ (see Fig. 2). For the wind scenario $\dot{M}/v_w \propto (1/L_{bol})^{(1/0.64)}$ (see Appendix A).

While giving less deep constraints, *Swift* observations have the advantage of being spread over a long time interval giving us the possibility to probe the CSM density over a wide range of radii. Integrating Eq. A8 in the time interval 1–65 days to match the *Swift* coverage (and using the 0.3–10 keV band) leads to $\dot{M}/v_w < 7 \times 10^{-8} (M_{\odot} \text{yr}^{-1}/100 \text{km s}^{-1})$ for $2 \times 10^{15} \lesssim R \lesssim 6 \times 10^{16}$ cm from the progenitor site²⁸. A similar value is obtained using the X-ray limit around maximum optical light, when the X-ray emission from IC is also expected to peak (Fig. 2²⁹).

3.2. ISM scenario

SN 2011fe might have exploded in a uniform density environment (ISM, $s = 0$). In this case, integrating Eq. A6 over the 0.5–8 keV energy range, the *Chandra* limit implies a CSM density $n_{CSM} < 166 \text{cm}^{-3}$ at 3σ confidence level for fiducial parameter values $p = 3$, $\epsilon_e = 0.1$, $E = 10^{51}$ erg and $M_{ej} = 1.4M_{\odot}$. This limit applies to day 4 after the explosion (or, alternatively to a distance $R \sim 4 \times 10^{15}$ cm, see Fig. 2). Integrating Eq. A6 over the time interval 1–65 days (and in the energy window 0.3–10 keV) the *Swift* upper limit implies $n_{CSM} < 800 \text{cm}^{-3}$ (3σ level), over a distance range $2 \times 10^{15} - 3 \times 10^{16}$ cm from the progenitor site³⁰. Around maximum light (days 8–38), we constrain $n_{CSM} < 770 \text{cm}^{-3}$ for distances $(1 \lesssim R \lesssim 3) \times 10^{16}$ cm. For an ISM scenario our constraints on the particle density $\propto (1/L_{bol})^{(1/0.5)}$ (see Appendix A).

Figure 3 (lower panel) shows how our *Chandra* limit compares to deep radio observations of SN 2011fe. We explore a wide parameter space to understand how a different photon effective temperature and/or electron power-law index p would affect the inferred density limit: we find $n_{CSM} \lesssim 150 \text{cm}^{-3}$ for $T_{eff} < 20000$ K and $2.2 \lesssim p \lesssim 3$. X-ray observations are less constraining than radio observations in the ISM case when compared to the wind case: this basically reflects the higher sensitivity of the synchrotron radio emission to the blastwave velocity, which is faster for an ISM-like ambient (for the same density at a given radius).

3.3. Implications

From the *Chandra* non detection we derive $\dot{M}/v_w < 2 \times 10^{-9} (M_{\odot} \text{yr}^{-1}/100 \text{km s}^{-1})$. This is the deepest limit obtained from X-ray observations to date and directly follows from (i) unprecedented deep *Chandra* observations, (ii) proximity of SN 2011fe coupled to (iii) a consistent treatment of the dynamics of the SN shock interaction with the environment (Appendix A). Before SN 2011fe, the deepest X-ray non-detection was reported for Type Ia SN 2002bo at a level of \sim

²⁸ Given the gentle scaling of the shock radius with wind density ($R \propto A^{-0.12}$, Eq. A7), these values are accurate within a factor 10 of \dot{M}/v_w variation.

²⁹ Note that in Fig. 2 the *Swift* limits are arbitrarily assigned to the linear midpoint of the temporal intervals. The limit on the ambient density is however calculated integrating the model over the entire time interval so that the arbitrary assignment of the "central" bin time has no impact on our conclusions.

³⁰ R has a very gentle ($\propto A^{-0.1}$, see Eq. A5) dependence on the environment density. The R values we list are representative of an ISM medium with a wide range of density values: $80 \lesssim n_{CSM} \lesssim 8000 \text{cm}^{-3}$.

$2 \times 10^{38} \text{ erg s}^{-1}$ (distance of 22 Mpc): using 20 ks of *Chandra* observations obtained 9.3 days after explosion, Hughes et al. (2007) constrained $\dot{M}/v_w \lesssim 10^{-4} (M_\odot \text{ yr}^{-1} / 100 \text{ km s}^{-1})$. This limit was computed conservatively assuming thermal emission as the leading radiative mechanism in the X-rays. Using a less conservative approach, other studies were able to constrain the X-ray luminosity from type Ia SNe observed by *Swift* to be $\lesssim 10^{39} \text{ erg s}^{-1}$ (Immler et al. 2006), leading to $\dot{M}/v_w \lesssim 10^{-7} (M_\odot \text{ yr}^{-1} / 100 \text{ km s}^{-1})$ (a factor ~ 100 above our result).

Our limit on SN 2011fe strongly argues against a symbiotic binary progenitor for *this* supernova. According to this scenario the WD accretes material from the wind of a giant star carrying away material at a level of $\dot{M} > 10^{-8} M_\odot \text{ yr}^{-1}$ for $v_w \lesssim 100 \text{ km s}^{-1}$ (see e.g. Seaquist & Taylor 1990; Patat et al. 2011a; Chen et al. 2011). We reached the same conclusion in our companion paper (Chomiuk et al. 2012) starting from deep radio observations of SN 2011fe. The radio limit is shown in Fig. 3 for the range of values $0.01 < \epsilon_B < 0.1$, with $\epsilon_B = 0.1$ leading to the most constraining limit (where ϵ_B is the post shock energy density fraction in magnetic fields). Historical imaging at the SN site rules out red-giant stars and the majority of the parameter space associated with He star companions (Li et al. 2011a, their Fig. 2): however, pre-explosion images could *not* constrain the Roche-lobe overflow (RLOF) scenario, where the WD accretes material either from a subgiant or a main-sequence star. In this case, winds or transferred material lost at the outer Lagrangian points of the system are expected to contribute at a level $\gtrsim 3 \times 10^{-9} (\dot{M}/M_\odot \text{ yr}^{-1}) (v_w/100 \text{ km s}^{-1})^{-1}$ if a fraction $\gtrsim 1\%$ of the transferred mass is lost at the Lagrangian points and the WD is steadily burning (see e.g. Chomiuk et al. 2012 et al and references therein). The real fraction value is however highly uncertain, so that it seems premature to rule out the entire class of models based on the present evidence. X-ray limits would be compatible with RLOF scenarios where the fraction of lost material is $< 1\%$ (for any $2.1 \lesssim p \lesssim 3$ and $5000 \text{ K} \lesssim T_{\text{eff}} \lesssim 20000 \text{ K}$, Fig. 3). However, from the analysis of early UV/optical data, Bloom et al. (2011) found the companion radius to be $R_c < 0.1 R_\odot$, thus excluding Roche-lobe overflowing red-giants and main sequence secondary stars (see also Brown et al. 2011).

X-ray non-detections are instead consistent with (but can hardly be considered a proof of) the class of double degenerate (DD) models for type Ia SNe, where two WDs in a close binary system eventually merge due to the emission of gravitational waves. No X-ray emission is predicted (apart from the shock break out at $t \ll 1$ day, see Sec. 5) and SN 2011fe might be embedded in a constant and low-density environment (at least for $R > 10^{14} \text{ cm}$). Pre-explosion radio HI imaging indicates an ambient density of $\approx 1 \text{ cm}^{-3}$ (Chomiuk et al. 2012) (on scales $R \gg 10^{14} \text{ cm}$), while our tightest limits in the case of an ISM environment are $n_{\text{CSM}} < 166 \text{ cm}^{-3}$. Our observations cannot however constrain the presence of material at distances in the range $10^{13} - 10^{14} \text{ cm}$ from the SN explosion: recent studies suggest that significant material from the secondary (disrupted) WD may indeed reside at those distances either as a direct result of the DD-merger (Shen et al. 2011) or as an outcome of the subsequent evolution of the system (Fryer et al. 2010).

Whatever the density profile of the environment, our findings are suggestive of a *clean* environment around SN 2011fe

for distances $2 \times 10^{15} < R < 5 \times 10^{16} \text{ cm}$. The presence of significant material at larger distances ($R \gtrsim 5 \times 10^{16} \text{ cm}$) cannot be excluded, so that our observations cannot constrain models that predict a large delay ($\gtrsim 10^5 \text{ yr}$) between mass loss and the SN explosion (see e.g. Justham 2011, Di Stefano et al. 2011 and references therein). Finally, it is interesting to note that the high-resolution spectroscopy study by Patat et al. (2011b) lead to a similar, *clean* environment conclusion: at variance with SN 2006X (Patat et al. 2007), SN 1999cl (Blondin et al. 2009) and SN 2007le (Simon et al. 2009), SN 2011fe shows no evidence for variable sodium absorption in the time period 8–86 days since explosion. In this context, a recent study by Sternberg et al. (2011) found evidence for gas outflows from Type Ia progenitor systems in at least 20% of cases.

Independent constraints on the circumstellar medium density around Type Ia SNe come from Galactic Type Ia supernova remnants (SNR): the study of Tycho’s SNR in the X-rays lead Katsuda et al. (2010) to determine a pre-shock ambient density of less than $\sim 0.2 \text{ cm}^{-3}$; the ambient density is likely $< 1 \text{ cm}^{-3}$ both in the case of Kepler’s SNR (Vink 2008) and in the case of SNR 0509-67.5 (Kosenko et al. 2008).

We emphasize that different type Ia SNe might have different progenitor systems as suggested by the increasing evidence of diversity among this class: we know that 30% of local SNe Ia have peculiar optical properties (Li et al. 2011b, Li et al. 2001). The above discussion directly addresses the progenitor system of SN 2011fe: our conclusions cannot be extended to the entire class of type Ia SNe.

4. LIMITS ON THE POST-SHOCK ENERGY DENSITY

While the IC emission model discussed here is primarily sensitive to CSM density, the associated radio synchrotron emission is sensitive to both the CSM density and ϵ_B (post shock energy density in magnetic fields). As a consequence, when combined with radio observations of synchrotron self-absorbed SNe, deep X-ray limits can be used to constrain the ϵ_B vs. ambient density parameter space (Chevalier & Fransson 2006; Katz 2012). This is shown in Fig. 4 for a wind (upper panel) and ISM (lower panel) environment around SN 2011fe: the use of the same formalism (and assumptions) allows us to directly combine the radio limits from Chomiuk et al. (2012) with our results. We exclude the values of $\epsilon_B < 0.02$ coupled to $\dot{M} > 2 \times 10^{-9} M_\odot \text{ yr}^{-1}$ for a wind medium, while $\epsilon_B < 0.1$ for any $\dot{M} > 5 \times 10^{-10} M_\odot \text{ yr}^{-1}$. In the case of an ISM profile, X-ray limits rule out the $\epsilon_B < 2 \times 10^{-3} n_{\text{CSM}} > 150 \text{ cm}^{-3}$ parameter space.

The exact value of the microphysical parameters ϵ_B and ϵ_e is highly debated both in the case of non-relativistic (e.g. SNe) and relativistic (e.g. Gamma-Ray Bursts, GRBs) shocks: equipartition ($\epsilon_B/\epsilon_e \sim 1$) was obtained for SN 2002ap from a detailed modeling of the X-ray and radio emission (Björnsson & Fransson 2004) while significant departure from equipartition ($\epsilon_e/\epsilon_B \approx 30$) has recently been suggested by Soderberg et al. (2011) to model SN 2011dh. The same is true for SN 1993J, for which $\epsilon_B/\epsilon_e \gg 1$ (Fransson & Björnsson 1998). In the context of relativistic shocks, GRB afterglows seem to exhibit a large range of ϵ_B and ϵ_e values (e.g. Panaitescu & Kumar 2001); furthermore, values as low as $\epsilon_B \sim 10^{-5}$ have recently been suggested by Kumar & Barniol Duran (2010) from accurate multi-wavelength modeling of GRBs with GeV emission. It is at the moment unclear if this is to be extended to the entire population of GRBs. On purely theoretical grounds, start-

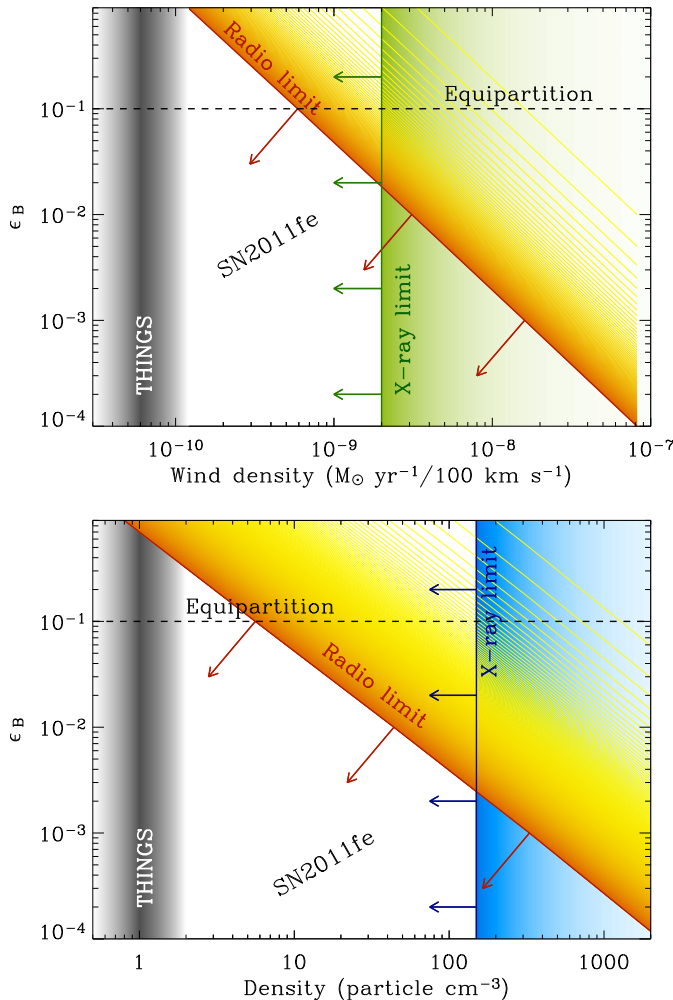


FIG. 4.— Constraints on the post-shock energy density in magnetic fields vs. ambient density parameter space as obtained combining the X-ray to the radio limits from Chomiuk et al. (2012). *Upper panel*: wind scenario. *Lower panel*: ISM environment. In both panels the grey area marks the pre-explosion density as measured from radio observations at the SN site (Chomiuk et al. 2012). A distance of 4×10^{15} cm has been used in the case of a wind medium. The horizontal dashed line marks equipartition ($\epsilon_B = \epsilon_e$) for the assumed $\epsilon_e = 0.1$. THINGS stands for “The HI Nearby Galaxy Survey” (Walter et al. 2008).

ing from relativistic MHD simulations Zhang et al. (2009) concluded $\epsilon_B \sim 5 \times 10^{-3}$; this result applies to GRB internal shocks, the late stage of GRB afterglows, transrelativistic SN explosions (like SN 1998bw, Kulkarni et al. 1998) and shock breakout from Type Ibc supernova (e.g. SN 2008D, Soderberg et al. 2008). It is not clear how different the magnetic field generation and particle acceleration might be between relativistic and non-relativistic shocks.

Figure 4 constitutes the first attempt to infer the ϵ_B value combining deep radio and X-ray observations of a Type Ia SN: better constraints on the parameters could in principle be obtained *if* X-ray observations are acquired at the SN optical maximum light. In the case of SN 2011fe we estimate that a factor ~ 10 improvement on the density limits would have been obtained with a *Chandra* observation at maximum light.

5. GAMMA AND X-RAY EMISSION FROM SHOCK BREAK OUT

Shock break out from WD explosions is expected to produce a short ($\approx 1 - 30$ ms) pulse with typical \sim MeV

photon energy, luminosity $\sim 10^{44}$ erg s $^{-1}$ and energy in the range $10^{40} - 10^{42}$ erg (Nakar & Sari 2011). Such an emission episode would be easily detected if it were to happen close by (either in the Milky Way or in the Magellanic Clouds), while SN 2011fe exploded ~ 6.4 Mpc away (Shappee & Stanek 2011). Given the exceptional proximity of SN 2011fe we nevertheless searched for evidence of high-energy emission from the shock break-out using data collected by the nine spacecrafts of the interplanetary network (IPN Mars Odyssey, Konus-Wind, RHESSI, INTEGRAL (SPI-ACS), *Swift*-BAT, Suzaku, AGILE, MESSENGER, and Fermi-GBM).

The IPN is full sky with temporal duty cycle $\sim 100\%$ and is sensitive to radiation in the range $20 - 10^4$ keV (Hurley 2010). Within a 2-day window centered on Aug 23rd a total of 3 bursts were detected and localized by multiple instruments of the IPN. Out of these 3 confirmed bursts, one has localization consistent with SN 2011fe. Interestingly, this burst was detected by KONUS, Suzaku and INTEGRAL (SPI-ACS) on August 23rd 13:28:25 UT: for comparison, the inferred explosion time of SN 2011fe is $16 : 29 \pm 20$ minutes, Nugent et al. 2011b. The IPN error box area for this burst is 1.4 sr. The poor localization of this event does not allow us to firmly associate this burst with SN 2011fe: from poissonian statistics we calculate a $\sim 10\%$ chance probability for this burst to be spatially consistent with SN 2011fe. A more detailed analysis reveals that SN 2011fe lies inside the KONUS-INTEGRAL triangulation annulus but outside the KONUS-Suzaku triangulation annulus. Furthermore, at the inferred time of explosion, SN 2011fe was slightly above the Fermi-GBM horizon, but no burst was detected (in spite of the stable GBM background around this time). We therefore conclude that there is no statistically significant evidence for a SN-associated burst down to the Fermi-GBM threshold (fluence $\sim 4 \times 10^{-8}$ erg cm $^{-2}$ in the 8-1000 keV band)³¹.

The early photometry of SN 2011fe constrains the progenitor radius to be $R_p \lesssim 0.02 R_\odot$ (Bloom et al. 2011). Using the fiducial values $E = 10^{51}$ erg, $M_{ej} = 1.4 M_\odot$, the shock break out associated with SN 2011fe is therefore expected to have released $E_{BO} \lesssim 3 \times 10^{41}$ erg over a time-scale $t_{BO} \lesssim 2$ ms with luminosity $L_{BO} \gtrsim 7 \times 10^{43}$ erg s $^{-1}$ at typical $T_{BO} \gtrsim 250$ keV (see Nakar & Sari 2011, their Eq. 29). At the distance of SN 2011fe, the expected fluence is as low as $\sim 5 \times 10^{-11}$ erg cm $^{-2}$ which is below the threshold of all gamma-ray observatories currently on orbit (the weakest burst observed by BAT had a 15-150 keV fluence of $\sim 6 \times 10^{-9}$ erg cm $^{-2}$). For comparison, the KONUS-Suzaku-INTEGRAL burst formally consistent with the position of SN 2011fe was detected with fluence $\sim 3 \times 10^{-6}$ erg cm $^{-2}$ and duration of a few seconds (peak flux of $\sim 4 \times 10^{-7}$ erg s $^{-1}$ cm $^{-2}$). If it were to be connected with the SN, the associated 3-sec peak luminosity would be $L \sim 2 \times 10^{45}$ erg s $^{-1}$ and total energy $E \sim 10^{46}$ erg (quantities computed in the 20-1400 keV energy band) which are orders of magnitudes above expectations.

For $t > t_{BO}$, the temperature and luminosity drop quickly (see Nakar & Sari 2011 for details): in particular, for $t > t_{NW}$ the emitting shell enters the Newtonian phase. For SN 2011fe we estimate $t_{NW} \sim 0.3$ s (Nakar & Sari 2011, their Eq. 30);

³¹ *Swift* is sensitive to fainter bursts: however it has a limited temporal coverage. We note that *Swift*-BAT was active and no burst was detected during the time window extending from 16:03:54 UT to 16:30:53 UT, implying a probability $> 50\%$ for a SN-associated burst with fluence above the *Swift* threshold and below the Fermi-GBM one to occur without being detected.

for $R_p \lesssim 0.02 R_\odot$ the luminosity at $t = 10 \times t_{\text{NW}}$ is $L(t_{\text{NW}}) \gtrsim 1 \times 10^{41} \text{ erg s}^{-1}$ with typical emission in the soft X-rays: $T(t_{\text{NW}}) \gtrsim 0.2 \text{ keV}$. At later times $L \propto t^{-0.35}$ (Nakar & Sari 2011) while T rapidly drops below the *Swift*-XRT energy band (0.3-10 keV). *Swift*-XRT observations were unfortunately not acquired early enough to constrain the shock break out emission from SN 2011fe. UV observations were not acquired early enough either: after ~ 1 hr the UV emission connected with the shock break out is expected to be strongly suppressed due to the deviation from pure radiation domination (e.g. Rabinak et al. 2011). It is however interesting to note the presence of a "shoulder" in the UV light-curve (Margutti & Soderberg 2011a) particularly prominent in the uvm2 filter for $t < 4$ days (see Brown et al. 2011, their Fig. 2) whose origin is still unclear (see however Piro 2012). A detailed modeling is required to disentangle the contribution of different physical processes to the early UV emission (and understand which is the role of the "red leak" -see e.g. Milne et al. (2010)- of the uvm2 filter in shaping the observed light-curve).

The collision of the SN ejecta with the companion star is also expected to produce X-ray emission with typical release of energy $E_x \sim 10^{46} - 10^{47} \text{ erg}$ in the hours following the explosion (a mechanism which has been referred to as the analog of shock break out emission in core collapse SNe, Kasen 2010). According to Kasen (2010), in the most favorable scenario of a red-giant companion of $M \sim 1 M_\odot$ at separation distance $a = 2 \times 10^{13} \text{ cm}$, the interaction time-scale is ~ 5 hr after the SN explosion and the burst of X-ray radiation lasts 1.9 hr (with a typical luminosity $\sim 6 \times 10^{44} \text{ erg s}^{-1}$): too short to be caught by our *Swift*-XRT re-pointing 1.25 days after the explosion. We furthermore estimate the high energy tail of the longer lasting thermal optical/UV emission associated to the collision with the companion star to be too faint to be detected either: at $t \sim 1.5$ days, the emission has $T_{\text{eff}} \lesssim 25000 \text{ K}$ and peaks at frequency $\nu \lesssim 3 \times 10^{15} \text{ Hz}$ (Eq. 25 from Kasen 2010). Non-thermal particle acceleration might be a source of X-rays at these times, a scenario for which we still lack clear predictions: future studies will help understand the role of non-thermal emission in the case of the collision of a SN with its companion star.

6. CONCLUSION

IC emission provides solid limits to the environment density which are *not* dependent on assumptions about the poorly constrained magnetic field energy density (i. e. the ϵ_B parameter; see also Chevalier & Fransson 2006 and Horesh et al. 2011). This is different from the synchrotron emission, which was used in our companion paper (Chomiuk et al. 2012) to constrain the environment of the same event from the deepest radio observations ever obtained for a SN Ia. The two perspectives are complementary: the use of the same assumptions and of a consistent formalism furthermore allows us to constrain the post-shock energy density in magnetic fields vs. ambient density parameter space (see Fig. 4). This plot shows how deep and contemporaneous radio and X-rays observations of SNe might be used to infer the shock parameters.

The IC luminosity is however strongly dependent on the SN bolometric luminosity: $L_{\text{IC}}(t) \propto L_{\text{bol}}(t)$. Here we presented the deepest limit on the ambient density around a type Ia SN obtained from X-ray observations. Our results directly benefit from: (i) unprecedented deep *Chandra* observations of one of the nearest type Ia SNe, coupled to (ii) a consistent treatment

of the dynamics of the SN shock interaction with the environment (Appendix A and Chomiuk et al. 2012), together with (iii) the direct computation of the SN bolometric luminosity from *Swift*/UVOT data.

In particular we showed that:

- Assuming a wind profile the X-ray non-detections imply a mass loss $\dot{M} < 2 \times 10^{-9} M_\odot \text{ yr}^{-1}$ for $v_w = 100 \text{ km s}^{-1}$. This is a factor of ~ 10 deeper than the limit reported by Horesh et al. 2011. This rules out symbiotic binary progenitors for SN 2011fe and argues against Roche-lobe overflowing subgiants and main sequence secondary stars *if* a fraction $\gtrsim 1\%$ of the transferred mass is lost at the Lagrangian points and the WD is steadily burning.
- Were SN 2011fe to be embedded in an ISM environment, our calculations constrain the density to $n_{\text{CSM}} < 160 \text{ cm}^{-3}$.

Whatever the density profile, the X-ray non-detections are suggestive of a *clean* environment around SN 2011fe, for distances in the range $\sim (0.2 - 5) \times 10^{16} \text{ cm}$. This is either consistent with the bulk of material (transferred from the donor star to the accreting WD or resulting from the merging of the two WDs) to be confined within the binary system or with a significant delay $\gtrsim 10^5 \text{ yr}$ between mass loss and SN explosion (e.g. Justham 2011, Di Stefano et al. 2011). Note that in the context of DD mergers, the presence of material on distances $10^{13} - 10^{14} \text{ cm}$ (as recently suggested by e.g. Fryer et al. 2010 and Shen et al. 2011) has been excluded by Nugent et al. (2011b) based on the lack of bright, early UV/optical emission.

We furthermore looked for bursts of gamma-rays associated with the shock break out from SN 2011fe. We find no statistically significant evidence for a SN-associated burst for fluences $> 6 \times 10^{-7} \text{ erg cm}^{-2}$. However, with progenitor radius $R_p < 0.02 R_\odot$ the expected SN 2011fe shock break out fluence is $\approx 5 \times 10^{-11} \text{ erg cm}^{-2}$, below the sensitivity of gamma-ray detectors currently on orbit.

The proximity of SN 2011fe coupled to the sensitivity of *Chandra* observations, make the limits presented in this paper difficult to be surpassed in the near future for type Ia SNe. However, the generalized IC formalism of Appendix A is applicable to the entire class of hydrogen poor SNe, and will provide the tightest constraints to the explosion environment *if* X-ray observations are acquired around maximum light (see Fig. 2) for Type I supernovae (Ia, Ib and Ic).

We thank Harvey Tananbaum and Neil Gehrels for making *Chandra* and *Swift* observations possible. We thank Re'em Sari, Bob Kirshner, Sayan Chakraborti, Stephan Immler, Brosk Russel and Rodolfo Barniol Duran for helpful discussions. L.C. is a Jansky Fellow of the National Radio Astronomy Observatory. R.J.F. is supported by a Clay Fellowship. KH is grateful for IPN support under the following NASA grants: NNX10AR12G (Suzaku), NNX12AD68G (Swift), NNX07AR71G (MESSENGER), and NNX10AU34G (Fermi). The Konus-Wind experiment is supported by a Russian Space Agency contract and RFBR grant 11-02-12082-ofi_m. POS acknowledges partial support from NASA Contract NAS8-03060.

REFERENCES

08. 1
- Björnsson, C.-I., & Fransson, C. 2004, *ApJ*, 605, 823
- Blondin, S., Prieto, J. L., Patat, F., Challis, P., Hicken, M., Kirshner, R. P., Matheson, T., & Modjaz, M. 2009, *ApJ*, 693, 207
- Bloom, J. S., et al. 2011, *ArXiv e-prints*, 1111.0966
- Boffi, F. R., & Branch, D. 1995, *PASP*, 107, 347
- Breeveld, A. A., et al. 2010, *MNRAS*, 406, 1687
- Brown, P. J., et al. 2011, *ArXiv e-prints*, 1110.2538
- . 2009, *AJ*, 137, 4517
- Chen, X., Han, Z., & Tout, C. A. 2011, *ApJ*, 735, L31
- Chevalier, R. A. 1982, *ApJ*, 258, 790
- Chevalier, R. A., & Fransson, C. 2006, *ApJ*, 651, 381
- Chevalier, R. A., Fransson, C., & Nymark, T. K. 2006, *ApJ*, 641, 1029
- Chomiuk, L., et al. 2012, *ArXiv e-prints*, 1201.0994
- Contardo, G., Leibundgut, B., & Vacca, W. D. 2000, *A&A*, 359, 876
- Curran, P. A., Evans, P. A., de Pasquale, M., Page, M. J., & van der Horst, A. J. 2010, *ApJ*, 716, L135
- Di Stefano, R., Voss, R., & Claeys, J. S. W. 2011, *ApJ*, 738, L1
- Dworkadas, V. V., & Chevalier, R. A. 1998, *ApJ*, 497, 807
- Eck, C. R., Cowan, J. J., Roberts, D. A., Boffi, F. R., & Branch, D. 1995, *ApJ*, 451, L53
- Felten, J. E., & Morrison, P. 1966, *ApJ*, 146, 686
- Foley, R. J., et al. 2012, *ApJ*, 744, 38
- Fransson, C., & Björnsson, C.-I. 1998, *ApJ*, 509, 861
- Frogel, J. A., Gregory, B., Kawara, K., Laney, D., Phillips, M. M., Terndrup, D., Vrba, F., & Whitford, A. E. 1987, *ApJ*, 315, L129
- Fryer, C. L., et al. 2010, *ApJ*, 725, 296
- Hancock, P. P., Gaensler, B. M., & Murphy, T. 2011, *ApJ*, 735, L35
- Hillebrandt, W., & Niemeyer, J. C. 2000, *ARA&A*, 38, 191
- Horesh, A., et al. 2011, *ArXiv e-prints*, 1109.2912
- Hughes, J. P., Chugai, N., Chevalier, R., Lundqvist, P., & Schlegel, E. 2007, *ApJ*, 670, 1260
- Hughes, J. P., Soderberg, A., & Slane, P. 2011, *The Astronomer's Telegram*, 3602, 1
- Hurley, K. 2010, *ISSI Scientific Reports Series*, 9, 235
- Iben, Jr., I., & Tutukov, A. V. 1984, *ApJS*, 54, 335
- Immler, S., et al. 2006, *ApJ*, 648, L119
- Justham, S. 2011, *ApJ*, 730, L34
- Kalberla, P. M. W., Burton, W. B., Hartmann, D., Arnal, E. M., Bajaja, E., Morras, R., & Pöppel, W. G. L. 2005, *A&A*, 440, 775
- Kasen, D. 2010, *ApJ*, 708, 1025
- Katsuda, S., Petre, R., Hughes, J. P., Hwang, U., Yamaguchi, H., Hayato, A., Mori, K., & Tsunemi, H. 2010, *ApJ*, 709, 1387
- Katz, B. 2012, *MNRAS*, 420, L6
- Kosenko, D., Vink, J., Blinnikov, S., & Rasmussen, A. 2008, *A&A*, 490, 223
- Kulkarni, S. R., et al. 1998, *Nature*, 395, 663
- Kumar, P., & Barniol Duran, R. 2010, *MNRAS*, 409, 226
- Li, W., et al. 2011a, *ArXiv e-prints*, 1109.1593
- Li, W., Filippenko, A. V., Treffers, R. R., Riess, A. G., Hu, J., & Qiu, Y. 2001, *ApJ*, 546, 734
- Li, W., et al. 2011b, *MNRAS*, 412, 1441
- Liu, J., Di Stefano, R., Wang, T., & Moe, M. 2011, *ArXiv e-prints*, 1110.2506
- Margutti, R., & Soderberg, A. 2011a, *The Astronomer's Telegram*, 3642, 1
- . 2011b, *The Astronomer's Telegram*, 3584, 1
- Matzner, C. D., & McKee, C. F. 1999, *ApJ*, 510, 379
- Milne, P. A., et al. 2010, *ApJ*, 721, 1627
- Nakar, E., & Sari, R. 2011, *ArXiv e-prints*, 1106.2556
- Nomoto, K. 1980, *Space Sci. Rev.*, 27, 563
- Nomoto, K., Thielemann, F.-K., & Yokoi, K. 1984, *ApJ*, 286, 644
- Nugent, P., Kim, A., & Perlmutter, S. 2002, *PASP*, 114, 803
- Nugent, P., Sullivan, M., Bersier, D., Howell, D. A., Thomas, R., & James, P. 2011a, *The Astronomer's Telegram*, 3581, 1
- Nugent, P. E., et al. 2011b, *ArXiv e-prints*, 1110.6201
- Panagia, N., Van Dyk, S. D., Weiler, K. W., Sramek, R. A., Stockdale, C. J., & Murata, K. P. 2006, *ApJ*, 646, 369
- Panaiteescu, A., & Kumar, P. 2000, *ApJ*, 543, 66
- . 2001, *ApJ*, 554, 667
- Patat, F., et al. 2007, *Science*, 317, 924
- Patat, F., Chugai, N. N., Podsiadlowski, P., Mason, E., Melo, C., & Pasquini, L. 2011a, *A&A*, 530, A63
- Patat, F., et al. 2011b, *ArXiv e-prints*, 1112.0247
- Perlmutter, S., et al. 1999, *ApJ*, 517, 565
- Piro, A. L. 2012, *ArXiv e-prints*, 1201.5398
- Rabinak, I., Livne, E., & Waxman, E. 2011, *ArXiv e-prints*, 1108.5548
- Riess, A. G., et al. 1998, *AJ*, 116, 1009
- Schlegel, D. J., Finkbeiner, D. P., & Davis, M. 1998, *ApJ*, 500, 525
- Sequist, E. R., & Taylor, A. R. 1990, *ApJ*, 349, 313
- Shappee, B. J., & Stanek, K. Z. 2011, *ApJ*, 733, 124
- Shen, K. J., Bildsten, L., Kasen, D., & Quataert, E. 2011, *ArXiv e-prints*, 1108.4036
- Simon, J. D., et al. 2009, *ApJ*, 702, 1157
- Soderberg, A. M., et al. 2008, *Nature*, 453, 469
- Soderberg, A. M., Kulkarni, S. R., Berger, E., Chevalier, R. A., Frail, D. A., Fox, D. B., & Walker, R. C. 2005, *ApJ*, 621, 908
- Soderberg, A. M., et al. 2011, *ArXiv e-prints*, 1107.1876
- Sternberg, A., et al. 2011, *Science*, 333, 856
- Vink, J. 2008, *ApJ*, 689, 231
- Walter, F., Brinks, E., de Blok, W. J. G., Bigiel, F., Kennicutt, Jr., R. C., Thornley, M. D., & Leroy, A. 2008, *AJ*, 136, 2563
- Wang, X., et al. 2009, *ApJ*, 697, 380
- Webbink, R. F. 1984, *ApJ*, 277, 355
- Whelan, J., & Iben, Jr., I. 1973, *ApJ*, 186, 1007
- Yost, S. A., Harrison, F. A., Sari, R., & Frail, D. A. 2003, *ApJ*, 597, 459
- Zhang, W., MacFadyen, A., & Wang, P. 2009, *ApJ*, 692, L40

APPENDIX

INVERSE COMPTON LUMINOSITY

Ambient electrons accelerated to relativistic speed by the SN shock are expected to upscatter optical photons from the SN photosphere to X-ray frequencies via Inverse Compton (IC), see e.g. Chevalier et al. (2006), Chevalier & Fransson (2006). Here we generalize Eq. (31) from Chevalier & Fransson (2006) for a population of relativistic electrons with arbitrary distribution $n_e(\gamma) = n_0\gamma^{-p}$ for $\gamma > \gamma_{\min}$, both for an ISM (Eq. A6) and a wind (Eq. A8) scenario.

Using the IC emissivity given by Felten & Morrison (1966), their Eq. 27, the IC luminosity reads:

$$\frac{dL_{\text{IC}}}{d\nu} = 2.1\sigma_{\text{T}}c \left(\frac{h}{3.6k} \right)^{\frac{3-p}{2}} R^2 n_0 \Delta R \rho_{\text{rad}} T_{\text{eff}}^{\frac{p-3}{2}} \nu^{\frac{1-p}{2}} \quad (\text{A1})$$

where $\rho_{\text{rad}}(t) = \frac{L_{\text{bol}}(t)}{4\pi R^2 c}$ is the energy density of photons of effective temperature T_{eff} which are upscattered to $\sim 3.6\gamma^2 k T_{\text{eff}}$; ΔR is the extension of the region containing fast electrons while R is the (forward) shock radius. The emission is expected to originate from a shell of shocked gas between the reverse and the forward shock which are separated by the contact discontinuity at R_c (Chevalier & Fransson 2006). For $\rho_{\text{SN}} \propto R^{-n}$ with $n = 10$ the forward shock is at $1.239R_c$ ($1.131R_c$) while the reverse shock is at $0.984R_c$ ($0.966R_c$) in the case of a wind (ISM) environment (Chevalier 1982). The fraction of the volume within the forward shock with shocked gas is 0.5 (0.4) corresponding to a sphere of radius $\Delta R \sim 0.8R$ ($\Delta R \sim 0.7R$) for an assumed wind (ISM) density profile.

If a fraction ϵ_e of the post-shock energy density goes into non thermal relativistic electrons, from $\int_{\gamma_{\min}}^{\infty} \gamma \cdot n_e(\gamma) d\gamma = 9/8 \epsilon_e \rho_{CSM} v_s^2$ we have:

$$n_0 = \frac{9(p-2)\epsilon_e \rho_{CSM} v_s^2 \gamma_{\min}^{(p-2)}}{8m_e c^2} \quad (\text{A2})$$

for $p > 2$. Combining Eq. A1 with Eq. A2, we obtain Eq. 1. The temporal evolution of L_{IC} directly depends on $L_{bol}(t)$; $T_{eff}(t)$; $v_s(t)$; $R(t)$ and $\gamma_{\min}(t)$. The properties of the SN and of its progenitor determine $L_{bol}(t)$, $T_{eff}(t)$ and the profile of the outer ejecta $\rho_{SN} \propto R^{-n}$. We assume $n \sim 10$ through out the paper (e.g. Chevalier & Fransson 2006). The environment sets the ρ_{CSM} profile, which we parametrize as $\rho_{CSM} \equiv A \cdot R^{-s}$. Both the SN explosion properties *and* the environment determine the shock dynamics: evolution of the shock radius $R(t)$, shock velocity $v_s(t)$ and, as a consequence $\gamma_{\min}(t)$. Under those conditions the shock interaction region can be described by a self-similar solution (Chevalier 1982) with the shock radius evolving as $R \propto t^{(\frac{n-3}{n-s})}$ which implies:

$$v_s(t) = \left(\frac{n-3}{n-s}\right) \frac{R(t)}{t} \quad (\text{A3})$$

The shock velocity directly determines γ_{\min} . From Soderberg et al. (2005), assuming that *all* electrons go into a power-law spectrum with spectral index p :

$$\gamma_{\min}(t) = \frac{9\epsilon_e}{8\eta} \left(\frac{m_p}{m_e}\right) \left(\frac{v_s(t)}{c}\right)^2 \left(\frac{\mu_i}{N_e/N_i}\right) \left(\frac{p-2}{p-1}\right) \quad (\text{A4})$$

where η is the shock compression parameter, N_e (N_i) is the electron (ion) number density and μ_i is the average number of nucleons per atom. We furthermore define $g(Z) \equiv \left(\frac{\mu_i}{N_e/N_i}\right)$. For Solar metallicity $g(Z_{\odot}) \approx 1.22$. In the following we assume $\eta \approx 4$ (Chevalier & Fransson 2006), $Z = Z_{\odot}$.

ISM scenario:

The self-similar solutions for the interaction of the SN ejecta with an ISM-like circumstellar medium ($s = 0$, $\rho_{CSM} \equiv A/R^s = A$) lead to (Chevalier 1982, Soderberg et al., in prep):

$$v_s(t) = 2.4 \times 10^9 \left(\frac{A}{\text{g/cm}^3}\right)^{-0.1} \left(\frac{E}{10^{51} \text{erg}}\right)^{0.35} \left(\frac{M_{ej}}{1.4M_{\odot}}\right)^{-0.25} \left(\frac{t}{s}\right)^{-0.29} \text{ cm s}^{-1} \quad (\text{A5})$$

where M_{ej} is the mass of the ejected material and E is the energy of the supernova explosion. Eq. A2, A3, A4 and A5, together with Eq. A1, predict an IC luminosity:

$$\frac{dL_{IC}}{d\nu} = f_{ISM}(p, Z) \epsilon_e^{p-1} \left(\frac{M_{ej}}{1.4M_{\odot}}\right)^{\frac{1-2p}{4}} \left(\frac{A}{\text{g cm}^{-3}}\right)^{(1.1-0.2p)} \left(\frac{E}{10^{51} \text{erg}}\right)^{(0.7p-0.35)} \left(\frac{t}{s}\right)^{(1.29-0.58p)} T_{eff}^{\frac{p-3}{2}} \nu^{\frac{1-p}{2}} \left(\frac{L_{bol}}{\text{erg s}^{-1}}\right) \frac{\text{erg}}{\text{sHz}} \quad (\text{A6})$$

with $f_{ISM}(p, Z) \approx 2.0 \times 10^7 (10^3)^{(1.1-0.2p)} (1.3 \times 10^{-11})^{\frac{3-p}{2}} \left(\frac{53.9}{2+p}\right)^{(p-2)} (p-2)^{(p-1)} g(Z)^{(p-2)}$. In the body of the paper A will be reported in (hydrogen) particles per cm^3 .

WIND scenario:

For $s = 2$ ($\rho_{CSM} \equiv A/R^2$) the self-similar solutions lead to (Chevalier 1982, Soderberg et al., in prep):

$$v_s(t) = 6.6 \times 10^{11} \left(\frac{A}{\text{g/cm}}\right)^{-0.12} \left(\frac{E}{10^{51} \text{erg}}\right)^{0.43} \left(\frac{M}{1.4M_{\odot}}\right)^{-0.31} \left(\frac{t}{s}\right)^{-0.12} \text{ cm s}^{-1} \quad (\text{A7})$$

Combining Eq. A2, A3, A4 and A7 with Eq. A1 we obtain:

$$\frac{dL_{IC}}{d\nu} = f_{WIND}(p, Z) \epsilon_e^{p-1} \left(\frac{M_{ej}}{1.4M_{\odot}}\right)^{(0.93-0.62p)} \left(\frac{A}{\text{g cm}^{-1}}\right)^{(1.36-0.24p)} \left(\frac{E}{10^{51} \text{erg}}\right)^{(0.86p-1.29)} \left(\frac{t}{s}\right)^{-(0.24p+0.64)} T_{eff}^{\frac{p-3}{2}} \nu^{\frac{1-p}{2}} \left(\frac{L_{bol}}{\text{erg s}^{-1}}\right) \frac{\text{erg}}{\text{sHz}} \quad (\text{A8})$$

with $f_{WIND}(p, Z) \approx 6.7 \times 10^{-7} 10^{(0.24p-1.36)} (1.3 \times 10^{-11})^{\frac{3-p}{2}} \left(\frac{5.6 \times 10^5}{2+p}\right)^{(p-2)} (p-2)^{(p-1)} g(Z)^{(p-2)}$.

Note that $\rho_{CSM} \equiv A/R^2 \equiv \dot{M}/(4\pi v_w R^2)$, so that $A = \dot{M}/(4\pi v_w)$, where \dot{M} and v_w are the mass loss rate and the wind velocity of the SN progenitor, respectively. In the body of the paper, for the wind scenario, we refer to A in terms of mass loss rate for a given wind velocity so that it is easier to connect our results to known physical systems.